2014 IEEE/RSJ International Conference on
Intelligent Robots and Systems (IROS 2014)
September 14-18, 2014, Chicago, IL, USA

High-throughput study of flapping wing aerodynamics for biological and robotic applications

Nick Gravish*, Yufeng Chen*, Stacey A. Combes and Robert J. Wood

Abstract— **The design of flapping wing robots and the study of flapping wing flyers requires a detailed knowledge of how wings interact with the surrounding fluid. However, the unsteady nature of fluid-structure interactions during flapping wing flight render analytical design of wing shapes and motion kinematics difficult. We propose that flapping wing micro aerial vehicle (MAV) design will benefit from a complimentary, data-driven approach in which wing shape, material properties, and stroke-kinematics may be varied rapidly. Here, we present a high-throughput experimental apparatus for fabrication and optimization of MAV wings for flapping flight. This apparatus incorporates the collection and analysis of multiple sensor modalities including force, electrical power, resultant fluid flow, and wing kinematics into the experiment control loop. This "analysis-in-the-loop" methodology enables multivariate optimization routines for flapping flight of unmanned aerial vehicles. We demonstrate the validity of this approach through optimization experiments on wing kinematics, fluid flow, lift and power consumption.**

I. INTRODUCTION

Recent advances in microrobotics such as the smart-composite manufacturing technique [1] and others have enabled the development and study of insect-scale micro aerial vehicles (MAV). The first stable free-flight of the Harvard RoboBee represents an advance in MAV control and fabrication [2]. However, sustained, energy-efficient flight in complex real-world environments requires further work to optimize wing kinematics, material properties, and flight energetics. To confront such a large design parameter space, we have developed an experimental apparatus that facilitates rapid acquisition and analysis of data on MAV and insect wing performance.

The aerodynamics of flapping flight are inherently unsteady [3]. Both biological and robotic studies of lift generation by flapping wings have highlighted several important lift-enhancing unsteady aerodynamic mechanisms such as a stable leading-edge vortex (LEV), added mass, wing-wing interactions, and wake capture (see [4] for a review). Modeling approaches based on the quasi-steady blade element method provide good estimates for the scaling of MAV flight metrics [5], but quasi-steady models can't account for unsteady aerodynamic phenomena which may be important in enhancing lift capacity or flight efficiency [6].

An alternative approach is to employ a high-throughput experiment in which many parameters can be systematically varied. This data-driven experimental approach can enhance the design process for wing shape, material properties and stroke kinematics for which there may be a multitude of suitable operating points. Furthermore, with the ability to rapidly vary parameters we can use the outcomes of previous trials to inform future parameters, thus optimizing the experimental design. We expect this process to accelerate the search for peak operating points for insect-scale flapping wing flight performance.

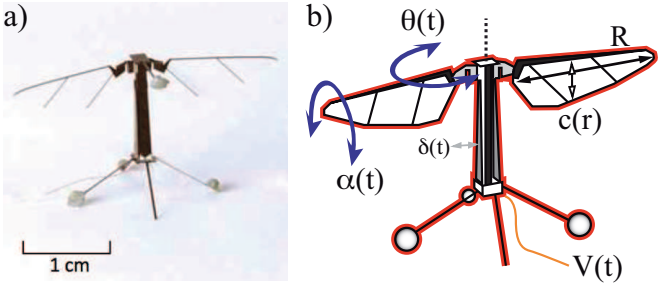

Fig. 1. Overview of Harvard RoboBee. a) The Harvard RoboBee (Photo courtesy of Pakpong Chirarattananon). b) Schematic of the Harvard RoboBee with design space parameters. Wing planform of radius R and chord function $c(r)$. Wing stroke angle, $\theta(t)$, is controlled by piezo-actuator displacement, $\delta(t)$, which in turn is controlled by an applied voltage, $V(t)$. Wing hinge angle, $\alpha(t)$ passively rotates under inertial and aerodynamic torques.

The RoboBee is actuated by a piezoelectric cantilever that flaps the wings along a horizontal stroke-plane (Fig. 1b, $\theta(t)$). While flapping, the wing rotates passively about the wing hinge [7], [8] with wing angle $\alpha(t)$ (Fig. 1b). The under actuated nature of the RoboBee wing, coupled with the unsteady aerodynamics of flapping flight, render a straightforward analytical approach to MAV wing design difficult. Recent theoretical and experimental studies have highlighted that flapping wing aerodynamics are sensitive to wing stiffness [9].

Previous optimization studies of flapping wing flight have been performed using quasi-steady numerical approaches [10] and experiments with a dynamically scaled robot [11], [12]. Dynamical scaling is the study of fluid forces and flow in systems that maintain geometric similarity and Reynolds number [13]. Dynamically scaled, flapping-wing robots such as Robofly [13] have provided valuable insights into unsteady flight aerodynamics. However, dynamically scaled experiments are limited in that wing material properties and flight energetics do not scale similarly. Thus, while this approach can help identify lift-enhancing stroke kinematics, optimum flight performance likely involves a number of additional

*Contributed equally to the work

Authors N.G., Y.C., and R.J.W., are with the Harvard Microrobotics Laboratory, authors N.G. and S.A.C. are with the department of Organismal and Evolutionary Biology Harvard University, Cambridge, MA 02138, USA gravish, yufengchen, rjwood@seas.harvard.edu, scombes@oeb.harvard.edu

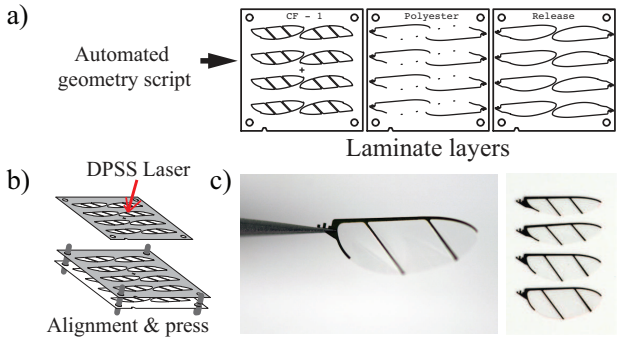

Fig. 2. Wing shape generation and fabrication. a) An automated program transforms wing planform into cut operations of carbon fiber and polymer laminates. b) Overview of the laminate cut operations. c) Laminates are cut with a DPSS laser and then aligned and bonded. d) Final wing (left) and four wings with varied planform (right).

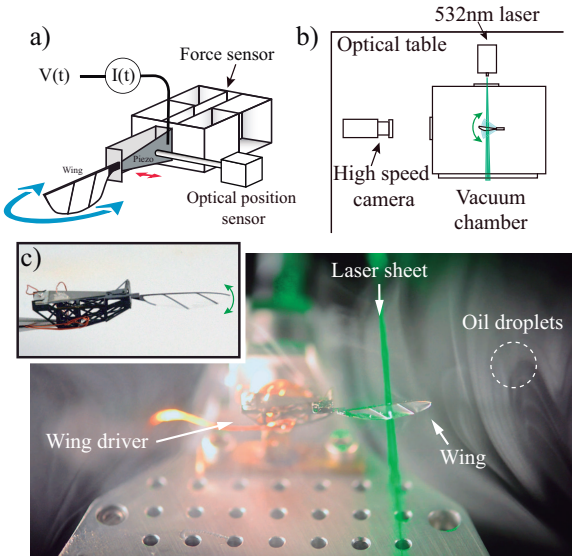

Fig. 3. Overview of experimental apparatus. a) Wing driver, fiber optic displacement sensor, and flapping wing orientation. The actuator is driven by a high-voltage signal, $V(t)$, and the current, $I(t)$, is monitored. b) Camera and laser setup. The wing-driver and sensors are enclosed in a vacuum chamber. c) Image of the wing-driver, force sensor, and laser. Inset shows wing driver. The vacuum chamber is seeded with buoyant oil particles that reflect laser light and illuminate fluid flow near the wing.

important metrics, including energy expenditure and force fluctuations. In addition, dynamical scaling does not allow simultaneous inertia matching, which is particularly important for studying passive wing rotation and corresponding energetics.

Previously we developed an experimental set up to measure the flapping kinematics and dynamics at the insect scale [7]. Here, we describe a data-driven experiment that integrates multiple simultaneous measurements of aerodynamic performance into one experimental system, which allows us to perform analysis in near real-time, thus placing analysis methods "in-the-loop." We describe the experiment design and test the efficacy of our "analysis in the loop" approach on two cases of optimization.

II. EXPERIMENTAL METHODOLOGY

The process of optimizing flight performance of MAVs such as the RoboBee consists of two components: 1) material and shape variation of wings and wing hinges, and 2) variation of actuation dynamics including voltage profile. To enable optimization studies we have developed a computer-automated wing layout method, and a flapping wing experimental apparatus with actuator control and multiple sensors monitored at or near real time.

A. AUTOMATIC WING PLANFORM AND SUPPORT GENERATION

We seek to study the effect of wing shape on flight performance during simple, controlled experiments in which a single shape parameter can be varied. Many parameters can be used to characterize wing morphology, including elliptical Fourier coefficients and eigenshape analysis [14]. Possibly the most well-known method of quantifying shape is that of Ellington [6] in which wing planform is described by the wing radius (R), a wing leading edge function, and a chord length function $c(r)$, which is a Beta distribution with two unique parameters. The aspect ratio of a wing, *AR*, is thus defined as the ratio of wing radius to $\max(c(r))$.

Previous wing shape variation studies required meanual generation in a professional CAD software. This process was both time consuming and inconsistent, since a human operator was in charge of hand determining fine details such as spar placement positions and fillet curves radii.

In this study, we have employed an automated algorithm to generate wing laser cutfiles from arbitrary wing shapes (Fig. 2). Once the outer contour of a wing is generated, leading edge and trailing edge wing frames are computed using local spline interpolation. The wing spars are structural support components that run from the wing leading edge to the wing trailing edge. They are equally spaced along the trailing edge and are tilted at a variable angle from the leading edge which we have chosen to be 45° in alignment with fiber direction. The wing is made of $0^\circ - 45^\circ - 0^\circ$ carbon fiber laminate to ensure high stiffness along the leading edge and the wing spar directions. Stress relief fillets are automatically placed at sharp corners. The wings used in our experiments are made of a carbon fiber structural frame and polyester membrane through the smart composite micro structure processes [15].

The mechanical construction of wings has been described previously [15]. Studies have indicated wing flexibility influences lift and drag production [9]. In our manufacturing process we can change wing flexibility by re-orienting the direction of carbon fiber laminate and by modifying the central fiber layer thickness. While it is straightforward to vary wing flexibility, we model the wing as a rigid plate and do not conduct flexibility studies in this paper.

With this wing generation technique we are able to rapidly lay out and manufacture wings while systematically varying planform shape parameters. In this study, we have

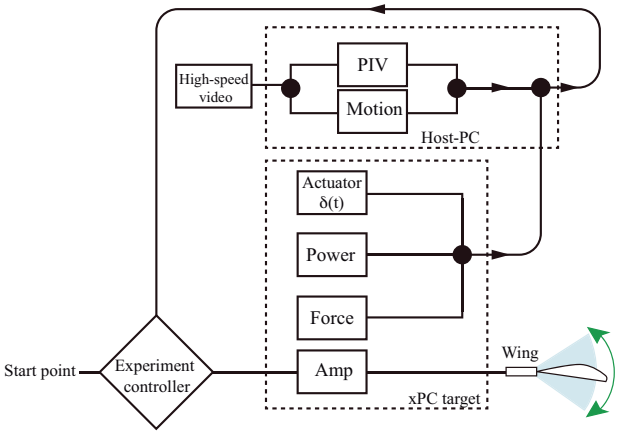

Fig. 4. Overview of the analysis-in-the-loop scheme.

constructed four wings of varied $c(r)$ (and thus varied AR) determined by the variation of a single parameter in the Beta distribution. While the traditional design process of a particular wing planform typically requires numerous hours of human labor, this algorithm automates this process thus allowing for fast design iterations.

B. FLAPPING WING EXPERIMENTS

We perform flapping wing experiments using a single active degree of freedom wing driver (Fig. 3). Wing motion is actuated by a piezoelectric bimorph actuator which is coupled to the wing through a four-bar transmission. The piezoelectric actuator is configured in a simultaneous drive mode with both a bias and signal voltage controlled by a high-voltage amplifier. The signal voltage, $V(t)$, drives the piezoelectric motion and the constant bias voltage held at $V_{bias} = \max(V(t)/2)$, sets the offset position. For the purposes of this experiment we constrain $V(t)$ to be sinusoidal with functional form $V(t) = V_A \sin(2\pi f t)$ where f is stroke frequency and V_A is stroke amplitude.

Wings are attached to the driver through a slot that holds them in place during experiments but allows for easy removal and replacement. Wings are actively rotated through a stroke angle, $\theta(t)$ (Fig. 1). The angle of attack, $\alpha(t)$, of the wing is not actively controlled, but instead rotates passively about the leading edge in response to inertial and aerodynamic loads. Wing hinge stiffness and range of motion may be modulated by varying hinge geometry. The passive rotation of the wing during flapping leads to either favorable or detrimental wing rotations, depending on the flapping kinematics, which in turn may lead to lift enhancement or reductions [7],

Experiments are performed within a vacuum chamber that is held at atmospheric conditions for these experiments. However, the internal pressure and gas within the chamber may be precisely controlled during experiments, representing a future area of research. To enable flow visualization, the chamber was filled with oil droplet particles generated from corn oil using a TSI atomizer.

III. SENSOR MEASUREMENTS

We use an array of sensors to monitor aerodynamic metrics during trials (Fig. 4), and experimental control and analysis are performed using Matlab and Simulink. An xPC target is called from the host PC computer with the Matlab real-time operating system runs Simulink, as well as the data acquisition and actuator controller program. The xPC target is called with a set of test parameters, such as frequency, amplitude, and waveform. The target then outputs the measured sensor readings to the host PC which integrates the sensor readings from the xPC and the high speed cameras.

The experimental pipeline thus consists of performing a measurement, recording the data to a stored location on the hard drive, and then operating on that data with analysis code. Based on the output of the analysis, we may then proceed to the next pre-determined experimental set-point or we may employ some controller to selectively choose the next experimental parameters. We call this method of rapid test, analyze, and iterate analysis-in-the-loop to echo similar concepts in control theory in which the system dynamics at study are supplied directly and in realtime to the the test platform.

A. MECHANICS MEASUREMENTS

The wing driver is connected directly to the input plate of a two-axis force sensor (Fig. 2). Wing lift and drag forces displace the parallel cantilever beams [16] along their direction of motion and we measure this displacement using two capacitive sensors (Physiks instrument). The sensor is constructed from 100 μm thick titanium and has a resonant frequency of $f = 630Hz$. In computational fluid dynamics simulations [17] we determined that frequency components of lift and drag are present up to the fourth harmonic of the flapping frequency. Since our system is designed to operate in the range of $\approx$100 Hz our sensor bandwidth is sufficient for these measurements. We low-pass filter the force sensor readings at $f = 500Hz$ to remove extraneous vibration and electrical noise from the force signal.

In addition to lift and drag, we measure the actuator displacement, $\delta(t)$, and the actuator power consumption (through current $I(t)$ and voltage $V(t)$ measurements). Actuator displacement is measured with a fiber optic displacement sensor (Philtec), which is directed at a reflective marker attached to the actuator surface near the transmission input. Comparing the actuator input displacement to the output wing rotation allows us to quantify the efficiency and dynamics of the transmission system.

We calculate the stroke-to-stroke power consumption of the actuator by measuring the current and voltage supplied to the piezoelectric actuator. Current in both the signal and bias channels is measured by isolation amplifiers (AD210J, Analog Devices) inserted in-line with the high-voltage drive signal. The total stroke power is defined as $P_{stroke} = f \int V(t)I(t) + V_{bias}I_{bias}(t)dt$, where the integral is evaluated over the steady-state portion of the experiment to avoid errors due to capacitive energy storage in the piezo-actuator.

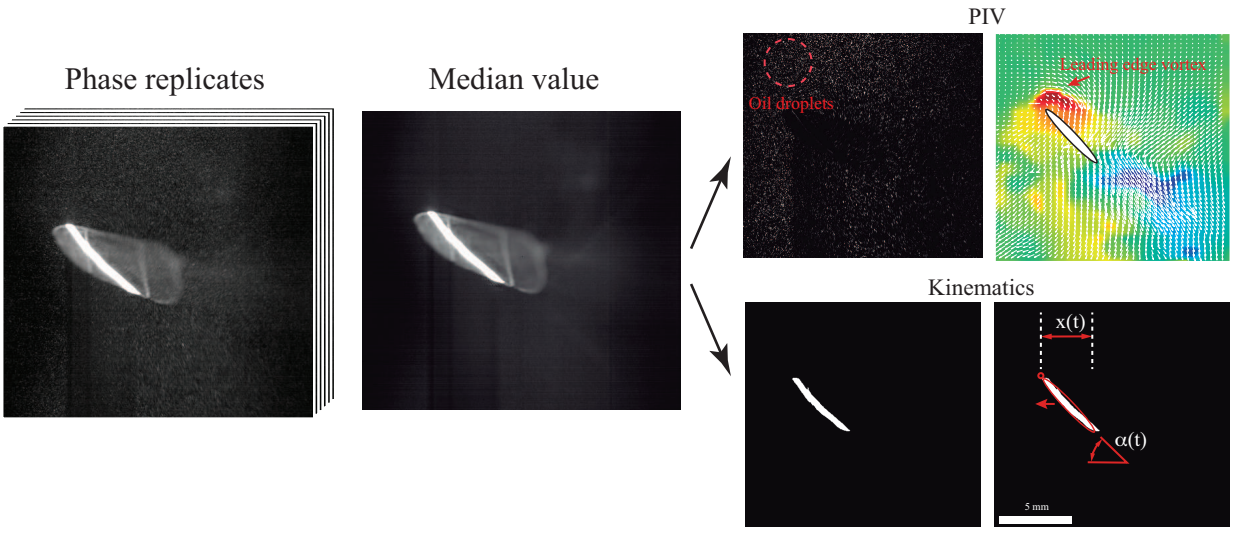

Fig. 5. Image processing steps from left to right. For each phase observation we collect the image replicates and construct a background image by computing the median value of each pixel over time. For PIV analysis (top middle and right) we subtract the median value background image from the current image at the same phase rendering only the oil droplets in the image. We construct the flow field and vorticity field as described in the text. Wing kinematics (bottom middle and right) are extracted by applying a set of morphological operations to the phase averaged background image. Stroke position and angle of attack are computed from linear regresssion of the binary image.

B. WING TRACKING

If the transmission were perfectly rigid and linear, measurement of actuator displacement would directly yield the wing stroke angle. However, flexible elements are incorporated into the wing transmission, and even more important the wing hinge rotates passively. To determine wing orientation and angle, we must thus capture high-speed video of the wing motion over time.

We use a high-speed Phantom v7.3 camera to record wing motion during experiments (See Fig. 2b for camera orientation and position). A 532 nm, 2W laser sheet illuminates a vertical plane positioned at mid-wingspan, normal to the camera sensor plane (Fig. 5). The laser sheet allows for visualization of fluid flow along the quasi two-dimensional plane of the laser. Image frame acquisition is triggered by the xPC target through digital pulses, so that frame acquisition and other sensor measurements are synchronized. To capture the high-speed motion of the particles and reduce motion blur we use a shutter time of $50\mu s$. We control acquisition parameters and video downloading through the Vision Research Matlab driver.

We captured 50 video frames per oscillation period and 40 oscillations. Each frame is captured at the same phase of oscillation. Our first step in video processing was to compute the background image for each phase of the oscillation from the replicate images at that phase. Background images were calculated as the median value of each (x,y) pixel location evaluated over time (Fig. 5). Using the background images we next performed two image analysis operations, digital particle image velocimetry and wing kinematics tracking.

Well-described fluid structures such as leading and trailing edge vortices are associated with aerodynamic force generation during flapping flight. To observe these features, we measure the fluid flow surrounding the flapping wing using the digital particle image velocimetry (PIV) technique [18]. We first subtracted from the ith image the phase averaged background image corresponding to that phase (Fig. 5). This operation resulted in an image with the wing removed and the fluid particles left. Velocity fields were determined from PIV by dividing the particle image into small patches on a square grid and registering the relative motion of objects in the image patches between times t and $t+\Delta t$. Object motion between the time steps is determined by locating the peak of the cross-correlation between the images. We use a Fourier-based approach to compute the correlation peak between PIV images in a custom Matlab routine [19].

Our PIV algorithm uses the series of high-speed camera images as inputs, and generates velocity vectors sampled on a grid of lattice dimensions 32×32 pixels as output. Measurements are then directly incorporated into the experimental pipeline. From the velocity vectors we are able to compute a number of metrics associated with aerodynamic performance including flow vorticity. Figure 5 shows a sample vorticity field and the associated velocity field for an oscillating wing. We observe a strong leading edge vortex (red) and a trailing edge vortex sheet (blue). Physically, the leading edge vortex corresponds to a low pressure region on the upper wing surface, which is responsible for high lift and drag observed in insect flight. This PIV study allow us to examine the connection between flapping kinematics, induced flow fields and associated dynamics. In this paper we compute the mean upstream suction velocity created by flapping wings.

In addition to revealing fluid flow, the laser sheet imaging system also illuminates a thin, bright, elliptical region of the

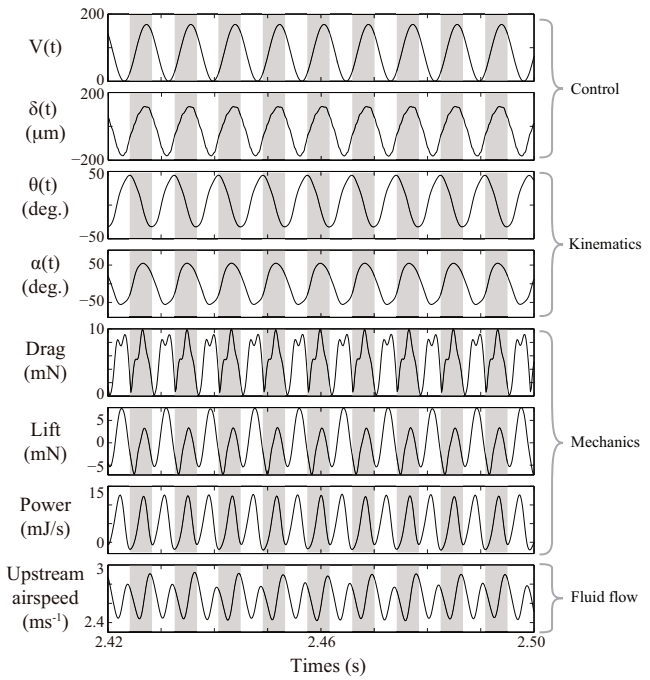

Fig. 6. Synchronous measurements from the sensors, camera, and electronics. Data are shown from a trial with $f = 120Hz$, and $V_A = 160\ V$. Gray shaded regions indicate downstroke while the white indicate upstroke.

wing (Fig. 5). By tracking the position and orientation of the wing-laser intersection we are able to track the wing stroke angle and hinge angle with high fidelity. Favorable wing kinematics are essential for lift generation [7]. We track the wing stroke position along the sheet laser plane, $x(t)$, and hinge angle, $\alpha(t)$. The tracking algorithm operates on the phase averaged background images and applies a series of morphological operations: we first threshold the image at a level of 150, then perform morphological closing and opening operations with a circular structuring element with radius 5 pixels to remove spurious points and fill holes in the wing blob. From the resultant binary image, we locate all connected components and retain only the largest component which is the wing-laser intersection (the ellipse in Fig. 5). We determine the wing centroid and orientation, $\alpha(t)$ and using standard geometry determine the horizontal distance of the wing leading edge from the wing root in the laser plane is $x(t)$ (Fig. 5). From $x(t)$ we compute the wing stroke angle $\theta(t) = \text{atan}(x(t)/l_0)$ where l_0 is the distance from wing-root to wing-laser intersection at $\theta = 0$.

C. EXAMPLES

In figure 6 we show example data from a measurement trial with amplitude of $V_A = 160$ V and frequency $f = 120\ Hz$. Here we show for the first time the actuation control, wing kinematics, fluid-mechanics, and fluid flow signals of a flapping MAV wing. These combined measurements represent a multivariate signature of flapping wing performance at a particular operating frequency and driving voltage pair.

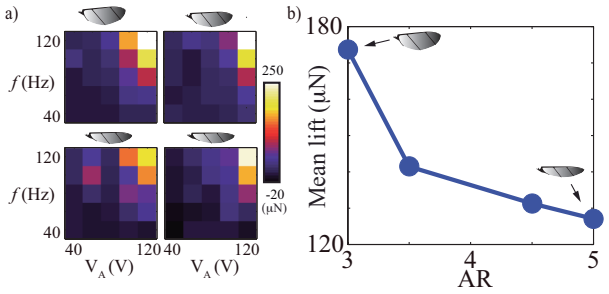

Fig. 7. Mean lift comparison for wings of different aspect ratio in the operational domain $40 < f < 120Hz, 40 < V_A < 120V$. a) shows the mean lift as functions of frequencies and driving voltages for wings with aspect ratio of $3, 3.5, 4.5$ and 5 (from upper left to lower right). b) compares mean lift of the wings at the operational point $110Hz, 110V$.

This set up allows us to rapidly evaluate flight performance at various operating points.

While aerodynamic efficiency depends on system driving frequency and voltage, it also depends on wing morphology and its inertial properties. Our automatic wing planform generation algorithm allows us to rapidly design and manufacture wings of different span, aspect ratio, and chord functions. From our combined wing generation and wing testing capabilities we can rapidly evaluate flight performance of multiple wing planforms. Figure 7a shows an example of mean lift as a function of driving voltage and frequency for four wings of different shape, which we characterize with the aspect ratio. Figure 7b compares the mean lift of different wings. Our analysis-in-the-loop experimental approach not only allows for rapid experiments with analysis on the fly, but also allows us to perform more advanced optimization experiments to explore wing performance.

IV. PROOF OF PRINCIPLE OPTIMIZATION

To test the utility of our analysis-in-the-loop approach we implemented an optimization scheme to identify desired operational points for sinusoidal wing flapping during hovering condition. We implemented a standard gradient descent algorithm which allows us to compare experimental optimization with theoretical predictions of performance. The optimization statement can be defined as

$$\underset{f,V_A}{\text{argmin}}\ g(f,V_A) \quad | \quad f \in \{f_{min}, f_{max}\}, V_A \in \{V_{min}, V_{max}\} \quad (1)$$

where f and V_A are the driving frequency and voltage amplitude which are restricted to some set of safe operating conditions. The objective functions returns a scalar value based on input variables. The gradient descent routine is performed as follows: given an initial guess, we sample the vicinity of the starting position to compute local gradient

$$\bar{\nabla} g = \begin{bmatrix} \frac{\partial g}{\partial f} \\ \frac{\partial g}{\partial V_A} \end{bmatrix} \quad (2)$$

and then move in the gradient direction with step size δx. The local step size is inversely proportional to the norm

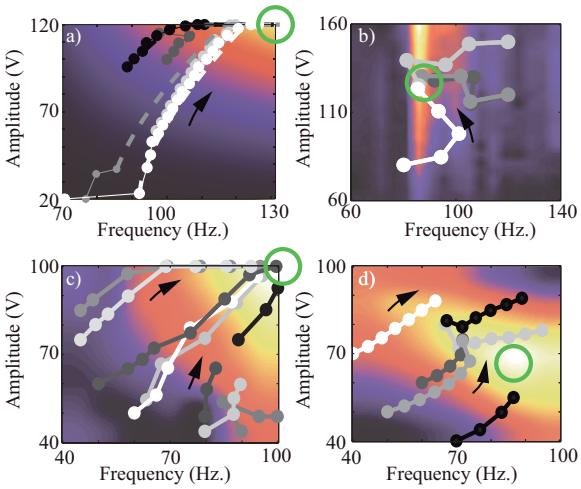

Fig. 8. Optimization results for gradient descent to maximize peak-peak drag force (a), maximize lift (b), maximize upstream fluid velocity (c), and tune for desired wing kinematics and power consumption set point (see text). Open green circles highlight desired maxima. Each circle represents an experiment and circle trajectories show the evolution of the optimization routine. Circles of different color correspond to different start points. Potential in (a) is generated from theoretical Af^2 function. Potential functions in (b-d) were generated in experiment, sampled in increments in 10 V and 10 Hz and interpolated.

of the local gradient, and it is restricted to a minimum value to reduce the number of steps taken. This algorithm terminates if $||\delta x||_2 < 1$. We have tested this algorithm on numerous polynomial objective functions and have found that convergence occurs typically within 10 steps. In actual experiment, we find the method converges after $4-15$ steps. This method only finds local extrema, hence multiple runs are needed to search for the global maximum of a complex objective function. For each optimization attempt, we repeat the algorithm several times and the initial guess of a subsequent run is placed away from previous optimization paths.

Depending on the specific application, the objective function we aim to maximize varies. Classical choices include maximizing mean lift or mean lift to drag ratio, which correspond to maximizing vehicle payload or endurance. Additionally, in our set up, since it is difficult to quantify transmission loss, it may be advantageous to minimize power input while satisfying a minimum mean lift threshold. As a first proof of principle for our analysis-in-the-loop method we performed four optimization experiments allowing actuator voltage and frequency to vary: 1) maximize peak-to-peak drag force which is important for performing controlled flight maneuvers (Fig. 8a), 2) maximize mean lift force (Fig. 8b), 3) maximize upstream suction velocity from PIV measurements (Fig. 8c), 4) seek an operating point which results in wing stroke amplitude of 40°, hinge amplitude of 17°, and stroke-to-stroke energy expenditure of 1 mJ (Fig. 8d).

The gradient descent optimization scheme to maximize drag force worked well for a variety of initial conditions (Solid circles in Fig. 8a). Trajectories matched our predictions (dashed lines in Fig. 8a) of functional form $V_A f^2$ which is shown in the background of Fig. 7a. For lift optimization we chose a wing and actuation parameter range which had a non-trivial potential gradient with optimum lift occurring for intermediate actuation frequency (Fig. 8b). All four trials converged to the correct frequency however the first-order optimization routine we implemented for these experiments was not robust enough to proceed to maximize amplitude.

To validate PIV analysis-in-the-loop we performed gradient descent optimization to maximize the suction velocity of flapping wings. We found that six out of nine trials successfully converged to the optimum amplitude, frequency combination (Fig. 8c). Three trials which had initial conditions of high frequency and low amplitude did not converge to the optimum (bottom right corner of Fig. 8c). Finally, we sought to determine the amplitude and frequency combinations which achieved wing kinematics of 40° stroke amplitude, 17° hinge amplitude, and which consumed stroke-to-stroke energy 1 mJ. This optimization routine incorporated synchronized high-speed video and actuator power measurements. All initial conditions converged towards the set-point operating conditions (green circle in Fig. 8d) however optimization routines terminated early in the flat portion of the potential field near the maxima. This last example highlights the need to implement higher order optimization schemes.

V. CONCLUSIONS AND FUTURE WORK

The goal of this paper is to present an experimental apparatus to enable data-driven engineering of actuator control, and wing design for the construction of next generation RoboBees. Flapping-wing organisms and robots are complex, non-linear dynamical systems. As such, the study of flapping-wing flight and the subsequent design principles derived from this should incorporate the simultaneous power-train, transmission, wing, and fluid flow dynamics. Previous experiments on lift generation by dynamically scaled flapping wings immersed in a high viscosity fluid do not capture the full device dynamics of a flapping wing robot or insect [13]. We posit that the exploration of wing inertia, flexibility, and energetic effects must be studied in systems at the relevant size scale of interest. At-scale experimental approaches such as the one described here are required to advance our understanding of MAV flight performance in real-world turbulent environments.

Given the mechanical and fluid dynamic complexities of insect-scale MAV flight, performing brute force parameter sweeps to search for desired operating points is infeasible. The full range of design-space parameters includes actuator variables (amplitude, frequency, waveform), wing shape and material, and actuator properties. Furthermore, the time consuming and human operator controlled process of designing wings has yielded sometimes inconsistent designs. Here we have describes an experiment which overcomes several major bottlenecks in the study and optimization of flapping-wing aerodynamic performance. Our beginning-to-end experimental methodology enables the optimization

of aerodynamic performance for flapping-wing flight. This system incorporates separate sensor modalities—force measurement, actuator power consumption, wing kinematics, and resultant fluid flow—into a single experiment. This data-driven design allows for rapid analysis of data, which can be incorporated into the experimental procedure enabling optimization studies which will greatly speed put the experimental design process.

Our experiments to optimize lift, drag, fluid flow, power consumption and kinematics given the variable parameters of amplitude and frequency serves as a proof of principle for future optimization studies. We envision that optimal flight performance depends on both energy efficiency and the generation of sufficient lift to perform flight maneuvers. Discovering the stroke parameters and mechanical design that contribute to optimum flight performance is a necessary step in equipping laboratory MAVs for the challenges of the real-world environment. Furthermore, flight in complex, natural environments may require alternative actuation strategies to overcome wind gusts [20], maneuver in confined spaces [21], or account for variable payloads [22]. The experimental framework we have described here paves the way for future studies of flight aerodynamics beyond the realm of hovering.

ACKNOWLEDGMENT

This work was partially supported by the National Science Foundation (award number CCF-0926148), and the Wyss Institute for Biologically Inspired Engineering. Dr. Gravish would like to acknowledge funding from the James S. McDonnell foundation. Any opinions, findings, and conclusions or recommendations expressed in this material are those of the authors and do not necessarily reflect the views of the National Science Foundation.

REFERENCES

[1] JP Whitney, PS Sreetharan, KY Ma, and RJ Wood. Pop-up book mems. *Journal of Micromechanics and Microengineering*, 21(11):115021, 2011.

[2] Kevin Y Ma, Pakpong Chirarattananon, Sawyer B Fuller, and Robert J Wood. Controlled flight of a biologically inspired, insect-scale robot. *Science*, 340(6132):603–607, 2013.

[3] Bin Liang and Mao Sun. Nonlinear flight dynamics and stability of hovering model insects. *Journal of The Royal Society Interface*, 10(85), 2013.

[4] Sanjay P Sane. The aerodynamics of insect flight. *The journal of experimental biology*, 206(23):4191–4208, 2003.

[5] JP Whitney and RJ Wood. Conceptual design of flapping-wing micro air vehicles. *Bioinspiration & Biomimetics*, 7(3):036001, 2012.

[6] CP Ellington. The aerodynamics of hovering insect flight. iii. kinematics. *Philosophical Transactions of the Royal Society of London. Series B, Biological Sciences*, pages 41–78, 1984.

[7] Alexis Lussier Desbiens, Yufeng Chen, and Robert J Wood. A wing characterization method for flapping-wing robotic insects. In *Intelligent Robots and Systems (IROS), 2013 IEEE/RSJ International Conference on*, pages 1367–1373. IEEE, 2013.

[8] JP Whitney and RJ Wood. Aeromechanics of passive rotation in flapping flight. *Journal of Fluid Mechanics*, 660(1):197–220, 2010.

[9] Liang Zhao, Qingfeng Huang, Xinyan Deng, and Sanjay P Sane. Aerodynamic effects of flexibility in flapping wings. *Journal of The Royal Society Interface*, 7(44):485–497, 2010.

[10] Gordon J Berman and Z Jane Wang. Energy-minimizing kinematics in hovering insect flight. *Journal of Fluid Mechanics*, 582(1):153–168, 2007.

[11] Scott L Thomson, Christopher A Mattson, Mark B Colton, Stephen P Harston, Daniel C Carlson, and Mark Cutler. Experiment-based optimization of flapping wing kinematics. In *Proceedings of the 47th Aerospace sciences meeting*, 2009.

[12] John David Anderson. *Fundamentals of aerodynamics*, volume 2. McGraw-Hill New York, 2001.

[13] Michael H Dickinson, Fritz-Olaf Lehmann, and Sanjay P Sane. Wing rotation and the aerodynamic basis of insect flight. *Science*, 284(5422):1954–1960, 1999.

[14] JD Crall, M Kovac, M Cornwall, RJ Wood, NE Pierce, and SA Combes. Shaping up: Aerodynamics and evolution of butterfly wing planform. In *INTEGRATIVE AND COMPARATIVE BIOLOGY*, volume 53, pages E42–E42. OXFORD UNIV PRESS INC JOURNALS DEPT, 2001 EVANS RD, CARY, NC 27513 USA, 2013.

[15] RJ Wood, S Avadhanula, R Sahai, E Steltz, and RS Fearing. Microrobot design using fiber reinforced composites. *Journal of Mechanical Design*, 130:052304, 2008.

[16] Rl J Wood, KJ Cho, and K Hoffman. A novel multi-axis force sensor for microrobotics applications. *Smart materials and structures*, 18(12):125002, 2009.

[17] Y. Chen and Robert J Wood. A computational tool to improve flapping efficiency of robotic insects. *ICRA*, 2014.

[18] CE Willert and M Gharib. Digital particle image velocimetry. *Experiments in fluids*, 10(4):181–193, 1991.

[19] JR Fienup and AM Kowalczyk. Phase retrieval for a complex-valued object by using a low-resolution image. *JOSA A*, 7(3):450–458, 1990.

[20] Stacey A Combes and Robert Dudley. Turbulence-driven instabilities limit insect flight performance. *Proceedings of the National Academy of Sciences*, 106(22):9105–9108, 2009.

[21] Daniel Mellinger and Vijay Kumar. Minimum snap trajectory generation and control for quadrotors. In *Robotics and Automation (ICRA), 2011 IEEE International Conference on*, pages 2520–2525. IEEE, 2011.

[22] Vojtech Vonasek, Martin Saska, and Libor Preucil. Motion planning for a cable driven parallel multiple manipulator emulating a swarm of mavs. In *Robot Motion and Control (RoMoCo), 2013 9th Workshop on*, pages 13–18. IEEE, 2013.